

The effect of cavitation on glacier sliding

BY CHRISTIAN SCHOOF

*Department of Earth and Ocean Sciences, University of British Columbia,
6339 Stores Road, Vancouver V6T 1Z4, Canada and
Mathematical Institute, University of Oxford, 24–29 St Giles’,
Oxford OX1 3LB, UK (cschoof@eos.ubc.ca)*

Basal sliding is one of the most important components in the dynamics of fast-flowing glaciers, but remains poorly understood on a theoretical level. In this paper, the problem of glacier sliding with cavitation over hard beds is addressed in detail. First, a bound on drag generated by the bed is derived for arbitrary bed geometries. This bound shows that the commonly used sliding law, $\tau_b = Cu_b^m N^n$, cannot apply to beds with bounded slopes. In order to resolve the issue of a realistic sliding law, we consider the classical Nye–Kamb sliding problem, extended to cover the case of cavitation but neglecting regelation. Based on an analogy with contact problems in elasticity, we develop a method which allows solutions to be constructed for any finite number of cavities per bed period. The method is then used to find sliding laws for irregular hard beds, and to test previously developed theories for calculating the drag generated by beds on which obstacles of many different sizes are present. It is found that the maximum drag attained is controlled by those bed obstacles which have the steepest slopes.

Keywords: glacier sliding; friction law; cavitation; Hilbert problem; contact problem

1. Introduction

The ability of glaciers to slide over their beds plays a crucial role in their dynamics. The motion of many of the world’s fastest flowing glaciers is dominated by sliding, while deformation within the bulk of the glacier ice contributes little to their overall discharge (see, for example, Kamb *et al.* 1985). Consequently, a sound understanding of the mechanics of glacier sliding is central to our ability to predict the behaviour of glaciers, especially those which can undergo rapid change by carrying large ice fluxes.

Recent interest has focused on the behaviour of deformable subglacial sediment and its effect on glacier sliding (see, for example, Tulaczyk *et al.* 2000*a*), while the classical theory considers ice sliding over a rigid, impermeable bedrock (see, for example, Cohen 2000; Fowler 1979, 1981, 1986; Gudmundsson 1997; Iken 1981; Kamb 1970; Lliboutry 1968, 1987; Morland 1976*a,b*; Nye 1969, 1970; Truffer & Iken 1998; Weertman 1957). Sliding over an undeformable bed is thought to occur when basal ice is near the melting point and a water film forms at the interface between ice and bed. This film is usually assumed to support insignificant shear stresses, allowing locally for free slip. Drag experienced by the glacier sole then arises because of undulations

on the glacier bed, which act as obstacles to ice flow. Ice motion over these obstacles occurs by a combination of viscous creep and regelation. In addition, there may be basal debris bridging the interfacial film, which will also contribute to basal drag (Fowler 1981; Morland 1976*b*; Schweizer & Iken 1992).

Provided the roughness wavelengths of the glacier bed are small compared with the thickness of ice above, boundary-layer theory (Fowler 1977, 1979, 1981) allows the flow of ice over bed obstacles to be parametrized in the form of a *sliding law*, which relates an averaged drag τ_b experienced by the glacier sole to the sliding velocity u_b ,

$$\tau_b = f(u_b). \quad (1.1)$$

Here, f is an increasing function of u_b , often taken to be of the form $f(u_b) = Cu_b^m$ with C and m positive constants. Strictly speaking, an explicit dependence on position along the bed ought also to be included in (1.1) to account for spatially varying bed roughness.

Relations of the form (1.1) constitute a nonlinear Robin-type boundary condition for the elliptic problem of determining the velocity field in the bulk of the glacier: τ_b is then the shear stress experienced by the bulk flow at the bed, which must be suitably smoothed for this purpose (Fowler 1981), while u_b is the tangential velocity of the bulk flow at the (smoothed) bed. It is worth pointing out that, unless lateral and longitudinal stresses in the bulk of the glacier are negligible, the basal shear stress τ_b cannot be equated with the geometrically defined driving stress (Paterson 1994, p. 240). In the general case, neither u_b nor τ_b can be prescribed independently, but form part of the solution to the ice flow problem. This is particularly important when the effect of cavitation is included in a sliding law, as we shall see below.

Lliboutry (1968) realized early on that the presence of high-pressure water at the beds of many glaciers could lead to the formation of water-filled cavities in the lee of bed obstacles, which would reduce the contact area between ice and bed and hence the drag experienced. In order to include the effect of cavitation on sliding, he proposed changing (1.1) to

$$\tau_b = f(u_b, N), \quad (1.2)$$

where the *effective pressure* N is the difference between the hydrostatic overburden of the ice p_i , due to the thickness of overlying ice, and basal water pressure p_c ,

$$N = p_i - p_c. \quad (1.3)$$

The smaller N is, the larger cavities should be, reducing the drag experienced by the glacier. Thus $f(u_b, N)$ should decrease with decreasing N , and many attempts to incorporate this effect into glacier dynamics models (see, for example, Pattyn 2002) rely on a heuristic power-law formulation

$$\tau_b = Cu_b^m N^n, \quad C, m, n > 0, \quad (1.4)$$

which was promoted by Budd *et al.* (1979), Bindshadler (1983), Fowler (1987) and Paterson (1994).

Crucially, relations of the form (1.4) allow arbitrarily high shear stresses τ_b to be generated at the bed, regardless of the value of N . This disagrees with the work of Iken (1981), who suggested that the quantity τ_b/N should satisfy an upper bound determined only by the geometry of the bed,

$$\tau_b/N \leq \tan \beta, \quad (1.5)$$

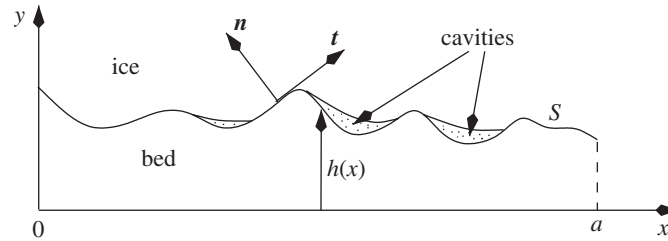


Figure 1. Illustration of the symbols used in the derivation of Iken's bound.

where β is the maximum up-slope angle between the bed and the mean flow direction. A bound of this type has profound implications for models of glacier flow: driving stresses in excess of $N \tan \beta$ cannot be balanced locally by basal drag (as would be predicted by the shallow-ice approximation (see Hutter 1983)) and longitudinal or lateral stresses must become important in ensuring force balance on the glacier. In particular, the bound implies that one cannot in general find a function g such that $u_b = g(\tau_b, N)$ exists for all combinations of τ_b and N (as we shall see later, $g(\tau_b, N)$ may in fact be multivalued for combinations of τ_b and N which admit such a function). Contrary to commonly held views in glaciology, one should therefore not think of a sliding law as determining sliding velocity u_b as a function of a given driving stress τ_b and effective pressure N , but as a relationship of the form (1.2) (which also encompasses 'solid' friction laws $\tau_b \propto N$ when $u_b > 0$).

Iken's derivation of the bound (1.5) assumes that the bed takes the form of a somewhat unrealistic 'tilted staircase', which may explain why it has been largely ignored in the literature. In this paper, we demonstrate how Iken's bound arises for quite general bed geometries. Motivated by the observation that (1.4) does not satisfy this bound, we then proceed to solve a model first used by Fowler (1986) to calculate actual sliding laws for sliding with cavitation over periodic bedrocks. The novelty here is that we are able to allow for any finite number of cavities per bedrock period, while Fowler's method only allowed for a single cavity. We are thus able to compute sliding laws for much more general and realistic bedrocks than was previously possible. We will also be able to shed light on the origins of sliding laws of the form (1.4), showing why they must be considered unphysical.

2. Iken's bound

The bound (1.5) arises for very simple reasons. Drag on the glacier sole is caused by high compressive (normal) stresses acting on the upstream sides of bed obstacles. As mean normal stress over the bed is controlled hydrostatically, high compressive stresses on the upstream sides of bed bumps are balanced by low compressive stresses on their lee sides. The latter may, however, not be able to drop below a critical value at which cavitation occurs. Consequently, once cavitation is initiated, it becomes more difficult to increase stresses on the upstream faces of bed obstacles, and drag generation is inhibited.

To see how this leads to the bound (1.5), consider an arc S of an undeformable, two-dimensional glacier bed in contact either with ice or a cavity fluid (liquid water, water vapour or air). We use a Cartesian coordinate system whose x -axis is aligned with the mean flow direction such that the projection of S onto the x -axis is $[0, a]$

(figure 1). $y = h(x)$ denotes the bed elevation at position x , and we assume that the first derivative $h'(x)$ is bounded and integrable.

Provided forces balance on the cavity fluid and its weight may be neglected, the force \mathbf{f} exerted by the bed on the overlying ice and cavity fluid equals the force exerted on the base of the ice over the same length of bed. Let \mathbf{n} and \mathbf{t} denote the upward-pointing normal and downstream-pointing tangent unit vectors to the bed, respectively. Using the usual compressive-negative sign convention for the stress tensor $\boldsymbol{\sigma}$ (note that we do not have to specify a rheology for ice or cavity fluid), \mathbf{f} can be written as

$$\mathbf{f} = (f_x, f_y) = - \int_S \boldsymbol{\sigma} \mathbf{n} \, ds = - \int_S (\mathbf{n} \cdot \boldsymbol{\sigma} \mathbf{n}) \mathbf{n} \, ds - \int_S (\mathbf{t} \cdot \boldsymbol{\sigma} \mathbf{n}) \mathbf{t} \, ds, \quad (2.1)$$

where $\boldsymbol{\sigma}$ is evaluated on S , ds is an element of the arc S , and (f_x, f_y) are the Cartesian components of \mathbf{f} . The notation $\boldsymbol{\sigma} \mathbf{n}$ is used for a contraction, $\sigma_{ij} n_j$ in component form, while ‘ \cdot ’ denotes the usual scalar product of two vectors.

The shear stress term $\mathbf{t} \cdot \boldsymbol{\sigma} \mathbf{n}$ vanishes if there is no tangential traction at the bed due to the presence of a water film. Defining local normal stress $\sigma_{nn} = \mathbf{n} \cdot \boldsymbol{\sigma} \mathbf{n}$, which we assume to be integrable, this leaves

$$f_x = \int_0^a \sigma_{nn} h'(x) \, dx, \quad f_y = - \int_0^a \sigma_{nn} \, dx, \quad (2.2)$$

where we have used $ds = [1 + h'(x)^2]^{1/2} dx$ and $\mathbf{n} = [1 + h'(x)^2]^{-1/2} (-h'(x), 1)$.

Assuming a is a suitable averaging distance (as discussed further below), standard two-dimensional basal sliding theory (e.g. Fowler 1981, 1986) calculates basal drag τ_b as an average upstream component of stress, $-f_x/a$. Similarly, the mean component of stress f_y/a perpendicular to the flow direction equals the hydrostatic overburden p_i , which is determined purely by glacier geometry. Thus

$$\tau_b = -\frac{1}{a} \int_0^a \sigma_{nn} h'(x) \, dx, \quad p_i = -\frac{1}{a} \int_0^a \sigma_{nn} \, dx, \quad (2.3)$$

Iken’s bound (1.5) now follows if we assume that compressive normal stress $-\sigma_{nn}$ cannot drop below a fixed critical value p_c , at which cavitation occurs. p_c is typically the water pressure in a subglacial drainage system, but could also be the triple-point pressure of water if parts of the bed are not well connected to the drainage system. Importantly, not all cavities have to exist at the same pressure, but it suffices for compressive normal stress to have a lower bound p_c .

Defining a local effective pressure $N_{\text{loc}}(x) = -\sigma_{nn} - p_c$, this criterion may be written as $N_{\text{loc}} \geq 0$. In terms of N_{loc} , (2.3)₁ can be expressed as

$$\begin{aligned} \tau_b &= \frac{1}{a} \int_0^a N_{\text{loc}}(x) h'(x) \, dx + \frac{1}{a} \int_0^a p_c h'(x) \, dx \\ &\leq \frac{\sup(h')}{a} \int_0^a N_{\text{loc}}(x) \, dx + \frac{p_c [h(a) - h(0)]}{a}, \end{aligned} \quad (2.4)$$

where we have made use of the fact that N_{loc} is positive, so

$$N_{\text{loc}}(x) h'(x) \leq N_{\text{loc}}(x) \sup(h'),$$

where \sup denotes the usual lowest upper bound. From $(2.3)_2$ and the definition of N_{loc} , the integral term on the second line can be recognized as the global effective pressure N ,

$$\frac{1}{a} \int_0^a N_{\text{loc}}(x) dx = p_i - p_c = N. \quad (2.5)$$

It remains to deal with the boundary term $p_c[h(a) - h(0)]/a$, which depends on the choice of averaging length a . The problem of having to define an averaging length has been discussed extensively in the glaciological literature (see, for example, Nye 1969). From a modern perspective, the averaging above can be viewed as an example of homogenization, with an inner length-scale given by bed roughness and an outer scale given by the length of the glacier (cf. Fowler 1981; Schoof 2002*b*). The standard assumption in that case (see, for example, Holmes 1995, ch. 5) is that the domain on the inner scale, and hence $h(x)$, is periodic with some arbitrary period a . Alternatively, and possibly more realistically, one can consider the asymptotic limit of large a (a much larger than the inner scale and much smaller than the outer scale) while requiring $h(a)$ to remain bounded (Schoof 2002*a*). In either case, the boundary term $p_c[h(a) - h(0)]/a$ vanishes. Equations (2.4) and (2.5) then combine to give

$$\tau_b \leq N \sup(h'), \quad (2.6)$$

which is the same as (1.5).

An extension of this derivation to three dimensions is straightforward, where h' in (2.6) must then be considered as the partial derivative of h with respect to the downstream coordinate. Complications to this simple bound arise primarily because there is likely to be tangential traction at a real glacier bed due to debris at the ice–bed interface. The existence of an upper bound on basal drag then depends on the interfacial friction law between ice and bed. Suffice it to say that a Coulomb friction law, which puts $\mathbf{t} \cdot \boldsymbol{\sigma} \mathbf{n} = -\mu \mathbf{n} \cdot \boldsymbol{\sigma} \mathbf{n}$ when $-\sigma_{nn} \geq p_c$ with μ a positive friction coefficient, leads to a bound for τ_b in terms of N , μ and bed geometry similar to (2.6).

3. A simple model for sliding with cavitation

Iken's bound demonstrates that sliding laws for beds with bounded slopes cannot be of the widely used form (1.4). This raises the question of what form a realistic sliding law which accounts for cavitation should take. To gain qualitative insight into this problem, we solve a model due to Fowler (1986) which considers ice of constant viscosity sliding over a periodic hard bed with small bed slopes and obstacle wavelengths which are small in comparison with ice thickness. The model is an extension of the classical Nye–Kamb theory (Kamb 1970; Nye 1969), covering the case of time-independent cavitation in the absence of regelation.

In common with other theories of basal sliding, Fowler's model assumes that forces on the glacier as a whole balance and that acceleration terms are negligible. Consequently, it does not deal with the 'unstable motion' envisaged by Iken (1981). This is motivated by the fact that this form of glacier flow, in which acceleration in the Newtonian sense becomes an important feature, does not occur very often. In most glaciers, longitudinal and lateral stress will ensure force balance if the driving stress locally exceeds the drag which the bed is able to generate (Raymond 1996; Schoof 2005).

A formal derivation of the dimensionless model may be found in Fowler (1986), and we do not repeat it here. In the half-space $y > 0$ of the (x, y) -plane we have the Stokes flow equations

$$\nabla^2 \mathbf{u} - \nabla p = \mathbf{0}, \quad \nabla \cdot \mathbf{u} = 0, \quad (3.1)$$

where $\mathbf{u} = (u, v)$ and p are variations about a constant mean flow velocity u_b (the sliding velocity) in the x -direction and about a hydrostatic pressure field, respectively.

At the bed (which to leading order is at $y = 0$ owing to the assumption of small bed slopes) we distinguish between contact areas between ice and bed, denoted by $x \in C'$, and cavities, denoted by $x \in C$. Labelling the endpoints of the j th cavity by b_j and c_j with $b_j < c_j < b_{j+1}$, we have

$$C = \bigcup_{j=-\infty}^{\infty} (b_j, c_j), \quad C' = \bigcup_{j=-\infty}^{\infty} (c_j, b_{j+1}). \quad (3.2)$$

If the period of the bed is a and there are n cavities per period, we further have $b_{j+n} = b_j + a$ and $c_{j+n} = c_j + a$.

Below, $h(x)$ again denotes the (scaled) elevation of the bed, now assumed twice Hölder continuously differentiable and periodic with period a , while $h_C(x)$ is the unknown shape of the cavity roof, and primes denote differentiation. $N = p_i - p_c$ is (scaled) global effective pressure. Boundary conditions may now be written as

$$u_y + v_x = 0, \quad v = u_b h'(x), \quad \text{on } y = 0, \quad x \in C', \quad (3.3)$$

$$u_y + v_x = 0, \quad p - 2v_y = -N, \quad v = u_b h'_C(x), \quad \text{on } y = 0, \quad x \in C. \quad (3.4)$$

$$u, v, p \rightarrow 0, \quad \text{as } y \rightarrow \infty, \quad (3.5)$$

where the subscripts ‘ x ’ and ‘ y ’ denote partial derivatives; thus $u_y = \partial u / \partial y$, etc. Further, u and v are required to be periodic in x with period a . The boundary conditions at the bed, (3.3) and (3.4), state that shear stresses vanish at the lower boundary of the ice, that this boundary is a steady material surface, and that normal stress at cavity roofs equals the cavitation pressure p_c (bearing in mind a hydrostatic contribution has been subtracted from p). The boundary conditions (3.5) arise as a result of matching velocities and pressure between the basal boundary layer and the outer bulk flow of the glacier (Fowler 1981; Schoof 2002*b*, Appendix A). Since the velocity perturbations \mathbf{u} vanish as $y \rightarrow \infty$ and the matching region is approached, the outer flow ‘sees’ u_b as the bed-parallel sliding velocity.

In addition to the boundary conditions above, there are the inequality constraints

$$h_C \geq h, \quad (p - 2v_y)|_{y=0} \geq -N, \quad (3.6)$$

stating that cavity roofs must be above the bed and that compressive normal stress at the bed cannot be less than the cavitation pressure. Further, we assume that cavity roofs join the bed at the cavity endpoints, so $h = h_C$ there. Lastly, drag τ_b , the object of our study, is determined by a relation analogous to (2.3)₁,

$$\tau_b = \frac{1}{a} \int_0^a (p - 2v_y + N)|_{y=0} h'(x) dx. \quad (3.7)$$

This equation results from matching shear stresses between the boundary layer and the outer flow. As pointed out by Fowler (1981), the assumption of small bed slopes

requires that the basal shear stress τ_b appears in the boundary layer problem only at second order, so that (3.7) does not conflict with the leading-order boundary conditions (3.5). It is straightforward to show, by integrating (3.1)₁ over the rectangle $0 < x < a$, $0 < y < R$, and using the divergence theorem in combination with (3.6) and (3.5) in the limit $R \rightarrow \infty$, that τ_b indeed satisfies Iken's (scaled) bound $\tau_b \leq N \sup_{x \in C'} h'(x) \leq N \max(h')$.

The main feature of the model is that the extent of cavitation is not known *a priori* but forms part of the solution. Fowler (1986) presented a method for solving the model which assumes that h is real analytic and that there is a single cavity per bed period. His results (which are reviewed in §5) therefore pertain only to quasi-sinusoidal beds, and their relevance to real glacier beds has been questioned on that basis (Fowler 1987; Lliboutry 1987). In the next section, we develop a method of solution which assumes only that h'' is Hölder continuous, and which crucially allows for any finite number of cavities per bed period. This allows us to study much more realistic beds than was previously possible.

4. Method of solution

Define the complex variable $z = x + iy$, and let

$$\left. \begin{aligned} \zeta &= \exp(i2\pi z/a), & \xi &= \exp(i2\pi x/a), \\ h_1(\xi) &= h'(x), & h_2(\xi) &= h''(x), & h_{2C}(\xi) &= h''_C(x). \end{aligned} \right\} \quad (4.1)$$

Note that h_1 , h_2 and h_{2C} are single-valued by the periodicity of the original problem. Further, let C (as a subset of the real axis in the z -plane) map to Γ and C' to Γ' under the transformation above; Γ and Γ' then each consist of n disjoint open arcs of the unit circle, and their location is not known *a priori*. The closure of their union is the unit circle itself (figure 2). Fowler (1986) and Schoof (2002*b*, ch. 3) show how the model in the previous section can be reduced to the following boundary-value problem for a function $G(\zeta)$ which is sectionally holomorphic in the ζ -plane cut along Γ' :

$$G^+(\xi) + G^-(\xi) = h_2(\xi), \quad \xi \in \Gamma', \quad (4.2)$$

$$G(0) = iN/(4u_b), \quad G(\infty) = -iN/(4u_b), \quad G(\zeta) = \overline{G(1/\bar{\zeta})}, \quad (4.3)$$

where an overbar denotes complex conjugation, and superscripts '+' and '-' indicate limits taken as ζ approaches the unit circle from the inside and outside, respectively. The function G arises through the use of complex variables in a stream function representation of the solution of the Stokes flow equations (3.1), as shown by Fowler (1986) and Schoof (2002*b*). On a technical note, we may add that Fowler's eqn (2.22) and Schoof's eqn (3.39) assume implicitly that the limits involved in taking boundary values and differentiating v commute. This is certainly true if $\partial v/\partial x$ is continuous near any given point on the boundary which does not coincide with one of the cavity endpoints. The latter can be verified straightforwardly using results in Muskhelishvili (1953, pp. 53–55) for the solution constructed below.

The unknown shape of the cavity roof and drag τ_b/N can be calculated in terms of G from

$$h_{2C}(\xi) = G^+(\xi) + G^-(\xi) = 2G(\xi), \quad \xi \in \Gamma, \quad (4.4)$$

$$\frac{\tau_b}{N} = -\frac{u_b}{\pi N} \int_{\Gamma'} \frac{G^+(\xi) - G^-(\xi)}{\xi} h_1(\xi) d\xi, \quad (4.5)$$

where integrals along Γ and Γ' will henceforth be taken as ξ traverses the unit circle in the anticlockwise direction. Note that (4.5) differs from Fowler's eqn (3.3)₃, which contains a typographical error.

Once Γ' is known, then equation (4.2) constitutes a classical Hilbert problem for the unknown function G . The general form of solutions to this problem is known (Muskhelishvili 1953, ch. 10), and once G has been found, drag τ_b can be calculated from (4.5).

The main challenge here is to determine the position of the cavity endpoints, and to choose the number and location of singularities in G . Both of these are constrained by the conditions (4.3) and the fact that (4.4) must generate a physically acceptable shape for the cavity roof. Without specifying the form of G , it is possible to see that the latter requirement imposes $2n - 1$ real constraints on the $2n$ positions of the cavity endpoints b_1, \dots, b_n and c_1, \dots, c_n . Consider the integral

$$\begin{aligned} I &= \frac{a}{2\pi i} \int_{\Gamma \cup \Gamma'} \frac{G^+(\xi) + G^-(\xi)}{\xi} d\xi \\ &= \sum_{j=1}^n \int_{b_j}^{c_j} h_C''(x) dx + \sum_{j=1}^n \int_{c_j}^{b_{j+1}} h''(x) dx \\ &= \sum_{j=1}^n [(h_C'(c_j) - h'(c_j)) + (h'(b_j) - h_C'(b_j))], \end{aligned} \quad (4.6)$$

where we have used $h'(b_{n+1}) = h'(b_1)$. By considering a three-term Taylor expansion of $h(x)$ and $h_C(x)$ near the cavity endpoints b_j and c_j , it is clear that the constraint $h_C(x) \geq h(x)$ for $b_j < x < c_j$, combined with the fact that $h(x) = h_C(x)$ at the cavity endpoints, requires that we have $h_C'(b_j) \geq h'(b_j)$ and $h_C'(c_j) \leq h'(c_j)$. From this it follows that $I \leq 0$, with equality holding if and only if $h_C'(b_j) = h'(b_j)$ and $h_C'(c_j) = h'(c_j)$ for all j .

It follows from the residue theorem and a version of Cauchy's theorem which applies to exterior regions (Muskhelishvili 1953, p. 63) that, if L is a closed contour encircling the origin,

$$\frac{1}{2\pi i} \oint_L \frac{G(\zeta)}{\zeta} d\zeta = \begin{cases} G(0) & L \text{ entirely inside the unit circle,} \\ G(\infty) & L \text{ entirely outside the unit circle,} \end{cases} \quad (4.7)$$

integrals being taken in the anticlockwise direction. Deforming the contour L to lie along the unit circle, indented in the appropriate direction around any points where G has integrable singularities (figure 2), the same conclusions still hold as G is then holomorphic between the original and deformed contours and continuous up to the deformed contour (Pollard 1923). By letting the radius of the indentations tend to

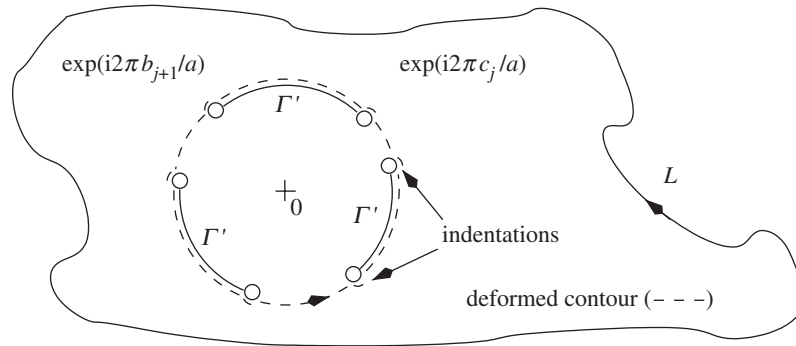


Figure 2. Schematic of the ζ -plane, showing the location of the branch cuts that make up Γ' as a heavy solid line with empty circles showing the branch points $\exp(i2\pi c_j/a)$, $\exp(i2\pi b_{j+1}/a)$. Also shown is a contour L as used in the derivation of (4.8).

zero in the usual way, one finds

$$\frac{1}{2\pi i} \int_{\Gamma \cup \Gamma'} \frac{G^+(\xi)}{\xi} d\xi = G(0), \quad \frac{1}{2\pi i} \int_{\Gamma \cup \Gamma'} \frac{G^-(\xi)}{\xi} d\xi = G(\infty). \quad (4.8)$$

Since $G(\infty) = -G(0)$ by (4.3), we obtain $I = 0$. Hence the conditions $h'_C(b_j) = h'(b_j)$ and $h'_C(c_j) = h'(c_j)$ must be satisfied for $j = 1, \dots, n$, stating that the cavity roof joins the bed tangentially at all cavity endpoints. Note that $I = 0$ implies that it is sufficient to impose only $n - 1$ of these conditions as constraints on the position of cavity endpoints, as the remaining one is satisfied automatically. Integrating both sides of (4.4) with respect to x , where $\xi = \exp(i2\pi x/a)$, these constraints may be expressed in the form

$$h'(b_j) + \int_{b_j}^{c_j} 2G(\exp(i2\pi x/a)) dx - h'(c_j) = 0, \quad j = 1, \dots, n - 1. \quad (4.9)$$

As G is real on Γ by (4.3)₃, this is easily seen to constitute $n - 1$ real constraints; in the case of $n = 1$, no constraints of this form arise, which is why they have no equivalent in Fowler's (1986) paper. n further constraints arise from requiring that the cavity roof does re-contact the bed at the cavity endpoints. Integrating both sides of (4.4) twice, these may be expressed as

$$h(b_j) + h'(b_j)(c_j - b_j) + \int_{b_j}^{c_j} 2(c_j - x)G(\exp(i2\pi x/a)) dx - h(c_j) = 0, \quad j = 1, \dots, n, \quad (4.10)$$

where we have made use of

$$\int_b^c \int_b^x f(x') dx' dx = \int_b^c (c - x)f(x) dx$$

for generic integrable f . Again, it is straightforward to see that these constraints are real.

A physically acceptable cavity roof therefore imposes $2n - 1$ real constraints on the position of the $2n$ cavity endpoints. One further constraint is needed, and this is supplied by the requirement that G satisfy the conditions (4.3). Here, we consider

only solutions of the form (see Muskhelishvili 1953, ch. 10)

$$G(\zeta) = \frac{\chi(\zeta)}{2\pi i} \int_{\Gamma'} \frac{h_2(\xi) d\xi}{\chi^+(\xi)(\xi - \zeta)} + G(\infty)\chi(\zeta), \quad (4.11)$$

where

$$\chi(\zeta) = \prod_{j=1}^n \left[\frac{\zeta - \exp(i2\pi b_{j+1}/a)}{\zeta - \exp(i2\pi c_j/a)} \right]^{1/2}, \quad (4.12)$$

and χ is holomorphic in the complex plane cut along Γ' , the branch taken behaving as $\chi(\zeta) \sim 1$ when $\zeta \rightarrow \infty$.

This choice of G has n integrable singularities, one at each downstream cavity endpoint (assuming $u_b > 0$). As we will indicate later, attempts to choose G with fewer endpoint singularities lead to an overdetermined problem for the position of cavity endpoints. The function G constructed above thus has the smallest possible number of singularities, and other choices with the same number of singularities differ from it only through the position of the singularities (and hence the choice of χ). Given that there must be n singularities, it is physically intuitive that there should be one per cavity. Equation (4.12) locates the singularities at the downstream cavity endpoints, in agreement with Fowler's (1986) solution. High contact stresses at downstream cavity ends were also suggested by Weertman & Birchfield (1982), and observed in the field by Vivian & Bocquet (1973). Furthermore, attempts to find solutions numerically with upstream endpoint singularities were unsuccessful, which explains why we persist with the definition of χ in (4.12).

The solution (4.11) satisfies the boundary condition (4.3)₂ automatically. To comply with the remaining conditions in (4.3) it is sufficient to impose

$$\overline{G(1/\bar{\zeta})} = G(\zeta).$$

Standard manipulation, taking care with the location of branch cuts and the branches chosen, shows that (cf. Schoof 2002b, pp. 49–51)

$$\overline{\chi\left(\frac{1}{\bar{\zeta}}\right)} = \frac{\chi(\zeta)}{\chi(0)} \quad \text{and} \quad \overline{\chi^+(\xi)} = \left[\overline{\chi\left(\frac{1}{\bar{\xi}}\right)} \right]^- = \frac{-\chi^+(\xi)}{\chi(0)}.$$

Furthermore, from $\xi = \exp(i2\pi x/a)$ with x real,

$$\bar{\xi} = \frac{1}{\xi} \quad \text{and} \quad d\bar{\xi} = \frac{-1}{\xi^2} d\xi.$$

After some manipulation, these observations allow $\overline{G(1/\bar{\zeta})}$ to be written as

$$\begin{aligned} \overline{G(1/\bar{\zeta})} &= \frac{\overline{\chi(1/\bar{\zeta})}}{-2\pi i} \int_{\Gamma'} \frac{h_2(\xi) d\bar{\xi}}{\overline{\chi^+(\xi)(\bar{\xi} - 1/\bar{\zeta})}} + \overline{G(\infty)} \overline{\chi(1/\bar{\zeta})} \\ &= \frac{\chi(\zeta)}{2\pi i} \int_{\Gamma'} \frac{h_2(\xi) d\xi}{\chi^+(\xi)(\xi - \zeta)} + \left\{ \frac{\overline{G(\infty)}}{\chi(0)} - \frac{1}{2\pi i} \int_{\Gamma'} \frac{h_2(\xi) d\xi}{\chi^+(\xi)\xi} \right\} \chi(\zeta), \end{aligned} \quad (4.13)$$

where we have also made use of the fact that $h_2(\xi)$ is real. Comparison with (4.11) and use of $\overline{G(\infty)} = iN/(4u_b)$ show that $\overline{G(1/\bar{\zeta})} = G(\zeta)$ requires

$$\frac{iN}{4u_b} - \frac{\chi(0)}{2\pi i} \int_{\Gamma'} \frac{h_2(\xi) d\xi}{\chi^+(\xi)\xi} + \frac{iN}{4u_b} \chi(0) = 0. \quad (4.14)$$

It remains to show that this constitutes a single real constraint, which can be accomplished by taking its complex conjugate. Manipulations analogous to those used to derive (4.14), and use of $|\chi(0)|^2 = 1$, show that the complex conjugate of the left-hand side of (4.14) can be reduced to a multiple of itself (with factor $-1/\chi(0)$), implying that its real and complex parts are linearly dependent (Schoof 2002*b*, p. 51). Hence (4.14) constitutes a single real constraint. Combined with (4.9) and (4.10), this is sufficient in principle to determine the position of the cavity endpoints c_1, \dots, c_n and b_1, \dots, b_n .

Having seen that G defined in (4.12) furnishes the correct number of constraints to determine the cavity endpoints, it is obvious that a solution with fewer singularities will lead to additional constraints and hence to an overdetermined problem. Indeed, it can be shown by analogy with the derivation of (4.14) that a solution with $n - \kappa$ singularities, where $-\kappa < 0$ is the index of the solution (Muskhelishvili 1953, ch. 10), has to satisfy $1 + \kappa$ real constraints in addition to (4.9) and (4.10), yielding a total of $2n + \kappa$ constraints for $2n$ cavity endpoints (Schoof 2002*b*, pp. 67–69). As there will in general be no solution in that case, a physically acceptable cavity roof shape therefore generally requires $\kappa \leq 0$ and at least n singularities.

A solution to the mathematical model stated in §3 therefore necessarily contains singularities, and the model must be missing some physical component or mechanism which ensures the regularity of solutions. One possibility is that the leading-order reduction of the ice flow domain to a half-space is responsible for the generation of singularities, which a solution of the full free boundary problem for sliding with cavitation may not exhibit. Another possibility is that the incorporation of regelation into the theory could alleviate the singularities: high contact stresses near the downstream cavity endpoints should lead to a significant lowering of the pressure melting point there, resulting in a large heat flux towards the area. This, in turn, should lead to significant melting, which implies that the neglect of regelation is no longer tenable close to the contact point.

Assuming that the effect of regelation is localized near the downstream cavity endpoints, we persist with the present model. A solution of the sliding problem can then be reduced to solving the constraints (4.9), (4.10) and (4.14) numerically, which is achieved using a backtracking line search modification of Newton's method (Dennis & Schnabel 1996, ch. 6). Once the location of cavity endpoints has been determined to a suitable accuracy, drag can be calculated from (4.5). Special care is needed when evaluating the integrals in (4.9), (4.10), (4.14) and (4.5). Many of the integrands involved have weak singularities, and the calculation of the boundary values of G requires a principal value integral to be evaluated. See Schoof (2002*b*, pp. 56–59) for further details of the numerical procedures used.

The development above assumes that the number n of cavities is known *a priori*, whereas it actually forms part of the solution. In particular, allowable values of n are determined by the fact that a solution of the sliding problem must satisfy the constraints (3.6); equation (3.6)₁ has already been used to derive the necessary conditions (4.9), but these are not sufficient to ensure that $h_C \geq h$ in the cavities. Both conditions must therefore be checked once a solution has been calculated. $h_C \geq h$ can easily be checked using (4.4), while (3.6)₂ becomes $-i(G^+(\xi) - G^-(\xi)) \geq 0$ on I' . If either inequality is violated, then a change in the number of cavities is indicated: either the calculated cavity roof makes contact with the bed, indicating

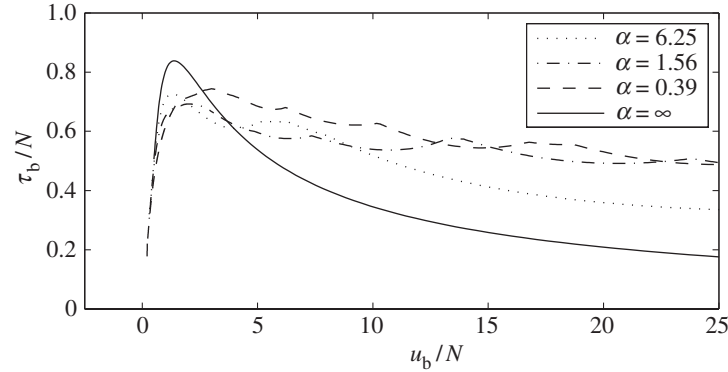


Figure 3. Sliding laws calculated for beds of the form (5.1). In each case, $a = 20\pi$ and $r_{\max} = 30$. Sliding laws are only shown after the onset of cavitation. Note that smaller α correspond to more irregular beds. $\alpha = \infty$ in the legend denotes a sinusoidal bed, which may be compared with the sliding law in fig. 3 of Fowler (1986). Note also that plotting u_b/N against τ_b/N (which corresponds to the ‘classical’ notion of a sliding law as determining u_b as a function of τ_b and N) simply amounts to flipping this graph on its side. The domain of τ_b/N is then clearly limited (as required by Iken’s bound), and the mapping $\tau_b/N \mapsto u_b/N$ for τ_b/N in that domain is in general multivalued.

the presence of an extra contact area, or the calculated normal stress drops below the critical pressure for cavitation, indicating the formation of a new cavity.

5. Results

From (4.2), (4.3) and (4.5), it is clear that the sliding law takes the form

$$\tau_b/N = f(u_b/N),$$

as was shown by Fowler (1986). Our method easily reproduces the form of $f(u_b/N)$ for a sinusoidal bed calculated by Fowler (see figure 3): initially, f increases as u_b/N increases, then reaches a global maximum and decreases again. This behaviour is associated with the migration of the contact areas between ice and bed to the tops of bed bumps at high u_b/N , as shown in fig. 4 of Fowler (1986). This migration, which happens simultaneously for all contact areas due to the simple periodic nature of the bed, causes the maximum bed slope in contact with ice to be reduced, and therefore leads to the drag τ_b/N decreasing. Fowler (1986) and Llibouty (1987) refer to this as the ‘drowning’ of bed roughness.

Figure 3 also shows sliding laws for a number of randomly generated irregular beds with ‘Gaussian’ Fourier spectra:

$$h(x) = \operatorname{Re} \left(\sum_{r=1}^{r_{\max}} \hat{h}_r \exp(i2\pi r x/a) \right), \quad \hat{h}_r = (\beta_r + i\gamma_r) K \exp(-\alpha(2\pi r/a - 1)^2). \quad (5.1)$$

Here α is a constant controlling the width of the spectrum (and hence the irregularity of the bed), while β_r and γ_r are random numbers between -1 and 1 and r_{\max} is some upper cut-off. The normalizing constant K is fixed so $\sum_{r>0} 8\pi^3 |\hat{h}_r|^2 r^3/a^3 = 1$, ensuring that $\tau_b/N = u_b/N$ before the onset of cavitation for each bed considered (Nye 1969).

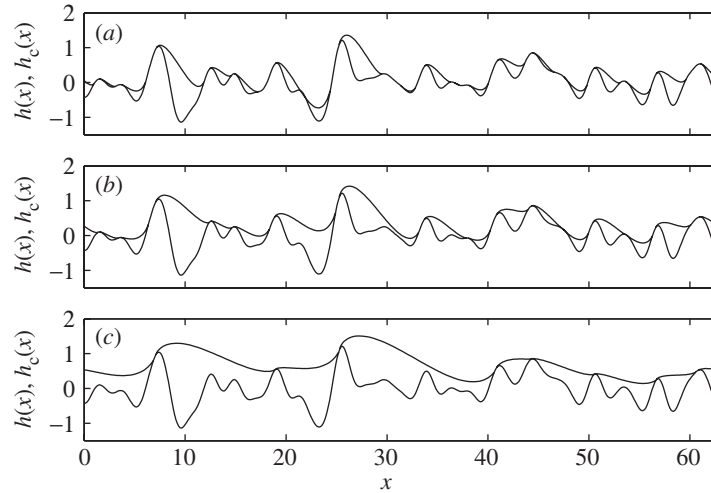


Figure 4. Cavity configurations for the bed with $\alpha = 0.39$ whose sliding law is shown in figure 3. Sliding velocities u_b/N are (a) 1.5, (b) 3, (c) 12. Contact areas extend over some fairly steep upstream faces even when $u_b/N = 12$.

Qualitatively, the sliding laws for these beds are similar to the sliding law for a sinusoidal bed, with τ_b/N rising initially as u_b/N increases, then reaching a global maximum, and finally decreasing again. The main difference between the sliding laws is that the maximum of τ_b/N is lower for irregular beds, and that the decrease in τ_b/N at higher u_b/N is less rapid. This is caused by the presence of more pronounced bed obstacles on the irregular beds. Steeper parts of these obstacles remain in contact with the ice at larger values of u_b/N , leading to a smaller decrease in drag (figure 4). Another feature which is present in the sliding laws for the irregular beds is a number of slope discontinuities in the graphs of τ_b/N against u_b/N ; these are associated with changes in the number of cavities present as u_b/N increases.

Importantly, the drop-off in τ_b/N is not related to the finite periodicity of the bed, but to the fact that contact areas again migrate to the tops of bed obstacles (although this does not happen simultaneously for all bumps). Furthermore, the maximum in τ_b/N is reached at similar values of u_b/N for all beds considered. This suggests that there may be a dominant obstacle size (presumably with wavelength of around 2π for each bed, owing to the form of $h(x)$ in (5.1)) which controls the form of the sliding law, and, in particular, the value of u_b/N at which the maximum of τ_b/N is attained.

Of course, real glacier beds do not have simple Fourier spectra of the type assumed above, but contain a wide spread of obstacle sizes (see, for example, Hubbard *et al.* 2000). This raises the question of whether a dominant obstacle size can be identified for more complicated beds. A direct answer to this problem is difficult to obtain, as our numerical method cannot resolve a wide spread of obstacle sizes. This difficulty has been addressed in part by Fowler (1987), who considers beds composed of obstacles with similar shapes but of (asymptotically) different sizes. His approach is to construct a scheme which recursively computes the drag generated by bumps of decreasing size, starting with some zeroth bump size which is subject to a far-field pressure $p_i = N + p_c$.

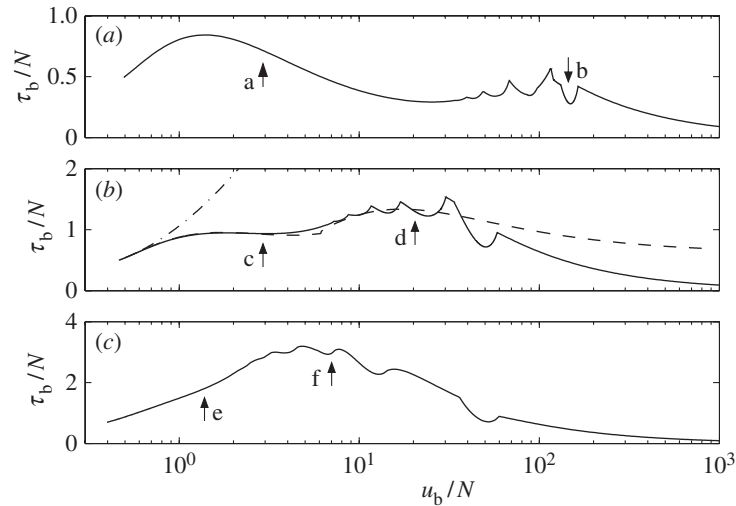


Figure 5. Sliding laws for beds of the form (5.2), plotted as solid lines. Note the logarithmic scale on the horizontal axis, and the different scales on the vertical axes. The labels next to the arrows indicate the panels in figure 6, which correspond to the values of u_b/N shown by the arrows. For each bed, $\lambda = 11$, while m is (a) 0.18, (b) 0.91, (c) 2.87. In (b), Fowler's (1987) approximation to the sliding law is also plotted as a dot-dashed line. Changing Fowler's eqn (3.14) as indicated in § 5 yields the sliding law shown as a dashed line in (b). This provides a reasonable approximation to τ_b/N except at large u_b/N .

To get some insight into the effect of bed obstacles of widely differing sizes, and to test whether Fowler's (1987) theory is likely to be successful, we calculate sliding laws for beds of the form

$$h(x) = m\lambda \cos(x/\lambda) + \sin(x), \quad (5.2)$$

which can be considered as a superposition of sinusoidal bumps of two 'asymptotically different' sizes provided the wavelength λ is large enough. (Alternatively, one could consider small λ , but we shall see below that the case of long wavelengths is more instructive.) Several examples are shown in figure 5. In panel (b), we also plot the sliding law predicted by Fowler's (1987) theory for the same bed. Clearly, this theory fails completely to reproduce the actual sliding law. In fact, reference to Fowler (1987) shows that his eqn (3.16) for calculating the total drag generated by the bed cannot be correct, even in an approximate sense. Specifically, this equation does not reproduce the correct sliding law for the case of a single bump size, owing to the presence of the term $1/s(\beta_r)$ on the right-hand side. It is possible to salvage Fowler's theory—the key to this turns out to be his eqn (3.14), which needs to be replaced by $N_r = s_r N_{r+1}$ (cf. figure 5b)—but doing so is beyond the scope of the present work.

The most important insight to be gained from figures 5 and 6, where the corresponding cavity configurations are plotted, is the following. Long-wavelength bumps (described in (5.2) by the first term on the right-hand side) only cause τ_b/N to continue increasing once short-wavelength bumps (described in (5.2) by the second term on the right-hand side) are significantly cavitated (or 'drowned out') if the *slope* m associated with the longer bumps is at least comparable with the unit slope associated with the shorter bumps. The wavelength corresponding to the steepest bumps

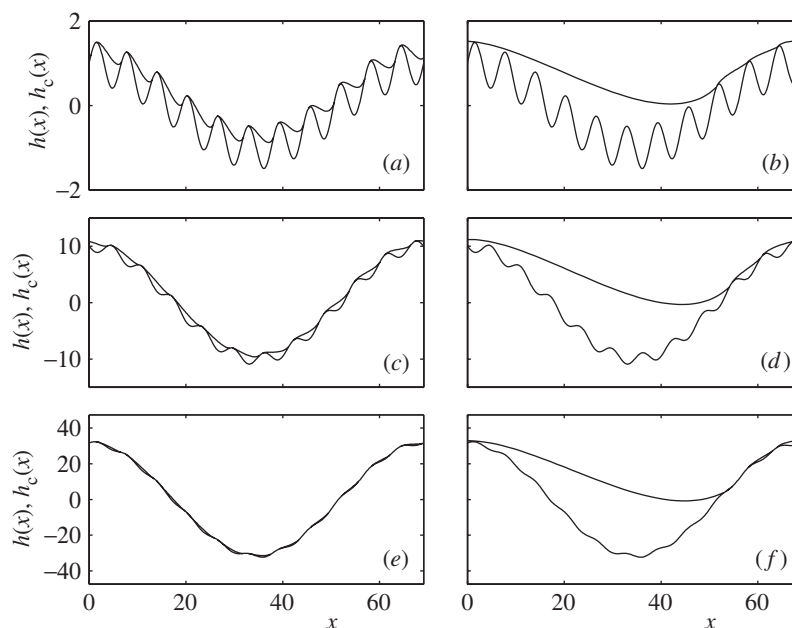


Figure 6. Cavity configurations for beds of the form (5.2), whose sliding laws are shown in figure 5. Each panel corresponds to the appropriately labelled arrow in figure 5. Note the different scales on the vertical axes. Panels (a) and (b) show the bed $m = 0.18$ at velocities u_b/N of (a) 3 and (b) 150. Note that the long bumps on this bed have a larger amplitude but smaller slope than the short obstacles. Panels (c) and (d) show the bed $m = 0.91$, in which short and long wavelength bumps have similar slopes, at velocities u_b/N of (c) 3 and (d) 20. Panels (e) and (f) show the bed $m = 2.87$, for which both obstacle sizes contribute equally to drag before cavitation, at velocities u_b/N of (e) 1.5 and (f) 7.

therefore appears to control the value of u_b/N at which the maximum of τ_b/N is attained. Panels (a) and (b) of figure 5 suggest that the sliding laws shown there consist essentially of two ‘humps’, one at low u_b/N and another, which has an uneven appearance, at higher u_b/N (this uneven appearance is due to changes in the number of cavities as u_b/N increases, as noted before). Arrows in figure 5 indicate the values of u_b/N at which the cavity roofs shown in figure 6 were calculated. Clearly, the first hump in the sliding laws in figure 5a,b corresponds to the short-wavelength obstacles becoming cavitated (figure 6a,c), while the second hump corresponds to large cavities forming in the lee of the longer obstacles (figure 6b,d). Crucially, the second hump is smaller than the first for the sliding law shown in figure 5a, which applies to a bed in which the longer-wavelength obstacles have a significantly lower slope than the shorter obstacles. By contrast, the second hump is slightly larger than the first in figure 5b, corresponding to a bed for which both obstacle sizes have similar slopes. The sliding law shown in figure 5c does not appear to consist of two humps. The cavity configurations shown in figure 6e,f indicate that this is the case because the longer obstacles become cavitated at only slightly larger values of u_b/N than the shorter ones. Again, τ_b/N continues to increase after the shorter obstacles have become cavitated, which can be attributed to the longer obstacles having steeper slopes.

This behaviour may be contrasted with the results of Fowler (1987), who obtains a power-law sliding (1.4), in which drag is always an increasing function of sliding velocity. Furthermore, this sliding law does not admit a bound of the form (2.6) and cannot therefore apply to a bed with bounded slopes. The reason for this turns out to be not so much Fowler's incorrect scheme for calculating the drag, but his prescription of a self-similar bed of the form

$$(\text{amplitude of } r\text{th bump size}) \propto (\text{wavelength of } r\text{th bump size})^{\alpha/2}, \quad (5.3)$$

where $\alpha > 2$ is a constant. There is some evidence that Fourier spectra obtained from exposed glacier beds can be fitted to power laws for limited ranges of wavenumbers (see, for example, Benoist 1979; Cuffey *et al.* 1999; Hubbard *et al.* 2000), but these fits do not hold at all wavelengths. For instance, fig. 5 of Hubbard *et al.* (2000) shows that a power-law fit to their data overestimates amplitudes at large wavelengths. Nevertheless, Fowler (1987) applies the relationship (5.3) to bed bumps of all length-scales, and also dispenses with a largest length-scale by integrating over wavelengths ranging to infinity (eqn (3.33) in his paper). The problem with doing so is that (5.3) states that the slope of bed obstacles increases with their wavelength. By integrating over wavelengths to infinity, Fowler assumes that there are infinitely long *and* steep bed bumps. This accounts for drag in his sliding law increasing without bound, but can hardly be considered physically realistic. Fowler's paper thus provides no physically sound basis for a hard-bed sliding law of the form (1.4).

6. Discussion

Iken's bound shows that basal drag satisfies a bound determined by effective pressure and bed geometry alone. This has potentially far-reaching implications for large-scale models of glaciers, which often rely on a lubrication (or *shallow ice*) approximation and equate the shear stress at the bed with the driving stress, which is prescribed in terms of ice thickness and surface slope (Fowler & Larson 1978; Hutter 1983; Morland & Johnson 1980). This may not, however, be possible. If effective pressure at the glacier bed drops rapidly through changes in basal drainage (as is typically associated with glacier surges (see, for example, Kamb *et al.* 1985)), while glacier geometry changes more slowly, then the driving stress may eventually exceed the drag τ_b which the bed is able to generate. In that case, the shallow-ice assumption of a driving stress balanced by drag at the bed *will* break down, and longitudinal and lateral stresses in the bulk of the glacier *must* become important if forces on the glacier are to balance locally. The mechanics of such glaciers may then be similar to ice streams underlain by weak till (Tulaczyk *et al.* 2000*b*), where lateral shear stresses rather than basal shear stress dominate force balance (Echelmeyer *et al.* 1994; Raymond 1996; Schoof 2005; Truffer *et al.* 2001).

Of course, the relevance of Iken's bound for real glacier beds may be questioned because they are likely to have at least some bed obstacles that have faces perpendicular to the flow direction, so the slope h' is unbounded. However, such obstacles may be rare in practice and it is unclear whether they would indeed allow unbounded amounts of shear stress to be supported at the bed. Unfortunately, the material in this paper does not provide a basis for studying the effect of bed obstacles perpendicular to the flow direction, as the derivation of the bound (2.6) and the model in §3 require bounded slopes.

Apart from showing how Iken's bound arises for arbitrary bed geometries with bounded slopes, we have extended Fowler's solution of the Nye–Kamb model with cavities to sufficiently smooth but otherwise arbitrary periodic beds. Our numerical solutions reveal that a finite bed period is not necessary to generate sliding laws in which τ_b/N has a global maximum and decreases at large values of u_b/N (figure 3); all that is required is a bounded bed slope and the existence of a dominant obstacle size. Put more precisely, if there is a spread of obstacle wavelengths, each associated with a typical slope, then those obstacles which have the steepest slopes control the velocity u_b/N at which drag τ_b/N reaches its maximum. We emphasize that this maximum is generally less than Iken's bound, an obvious exception being the 'tilted staircase' bed used by Iken (1981); here τ_b/N does attain Iken's bound once cavities extend over all the downstream faces of the 'staircase'.

These results must be contrasted with the conjectures of Fowler (1987) and Lliboutry (1987), who argued that drag should not attain a maximum but increase without bound because, regardless of velocity, there should always be 'larger' obstacles present which are able to provide increased drag. As shown in § 5, this only holds true if these larger obstacles also have steeper slopes than the obstacles that have already become cavitated.

Of practical interest is the dimensional value of u_b/N at which τ_b/N reaches its maximum; this problem is obscured somewhat by the fact that we are dealing with dimensionless models in §§ 3–5. Given a dimensional wavelength λ_{\max} for the dominant bumps, and a typical slope m_{\max} , typical deviatoric normal stresses σ generated by flow over these bumps are of the order $\sigma \sim m_{\max}\eta u_b/\lambda_{\max}$ (see Fowler (1981, 1986, 1987) for a discussion of the scalings involved), where η is ice viscosity and σ and u_b are dimensional. Stress σ must be comparable with dimensional effective pressure N when bumps at this size begin to cavitate. Hence $u_b/N \sim \lambda_{\max}/(m_{\max}\eta)$ when drag τ_b/N attains its maximum.

Ice typically does not have constant viscosity, and it is tempting to extend our discussion to a more general Glen's law rheology. With such a rheology, we have $A\sigma^n \sim m_{\max}u_b/\lambda_{\max}$, where A and n are the usual parameters for Glen's law (Paterson 1994, ch. 5). Again requiring $\sigma \sim N$ leads to

$$u_b/N^n \sim (\lambda_{\max}A)/m_{\max} \doteq A_0 \tag{6.1}$$

as the order of magnitude of u_b/N^n at which τ_b/N should reach its maximum. This is, of course, only an ad hoc generalization to the case of a nonlinear rheology, and strictly speaking only applies when $n = 1$.

We conclude by constructing a simple analytical sliding law which incorporates the qualitative results of this paper. At low velocities and high effective pressures, before the onset of cavitation, τ_b is independent of effective pressure. Ignoring regelation, the sliding law should then behave as $\tau_b \propto u_b^{1/n}$, where n is the exponent in Glen's law (see, for example, Fowler 1981). At higher velocities or lower effective pressures, when there is significant cavitation, τ_b/N attains a maximum when $u_b/N^n \sim A_0$, where A_0 is defined in (6.1). Furthermore, this maximum must satisfy Iken's bound (2.6). At even higher velocities or lower effective pressures, τ_b/N may be expected to decrease again. However, the results shown in figure 3 indicate that this decrease is slow. For the purpose of constructing a simple sliding law, it may be preferable to let τ_b/N tend to a limit from below for $u_b/N^n \gtrsim A_0$, rather than having τ_b/N attain a

maximum and decrease again. One of the simplest relations which incorporates these features takes the form

$$\frac{\tau_b}{N} = C \left(\frac{\Lambda}{\Lambda + \Lambda_0} \right)^{1/n}, \quad \Lambda = \frac{u_b}{N^n}, \quad (6.2)$$

where the constant C is less than the maximum bed slope. For $n = 1$, this reproduces the qualitative features of the sliding laws shown in figure 3 fairly well, provided we are not concerned with the case of very large u_b/N . The generalization to a nonlinear rheology, and specifically assuming that τ_b/N is a function of u_b/N^n , should at best be viewed as heuristic. However, one should note that this sliding law is essentially the same as proposed by Fowler (1987, fig. 6) for self-similar beds with an upper wavelength cut-off. Use of this sliding law would, at least, be preferable to a power-law of the form (1.4).

This work was supported by a UK Engineering and Physical Sciences Research Council doctoral studentship, the Garside Senior Scholarship at Corpus Christi College, Oxford, and a Killam Postdoctoral Research Fellowship at the University of British Columbia. Discussions with Andrew Fowler and Garry Clarke as well as the helpful comments of the two referees are gratefully acknowledged.

References

- Benoist, J.-P. 1979 The spectral power density and shadowing function of glacial microrelief at the decimetre scale. *J. Glaciol.* **23**(89), 57–66.
- Bindschadler, R. 1983 The importance of pressurized subglacial water in separation and sliding at the glacier bed. *J. Glaciol.* **29**(101), 3–19.
- Budd, W. F., Keage, P. L. & Blundy, N. A. 1979 Empirical studies of ice sliding. *J. Glaciol.* **23**(89), 157–170.
- Cohen, D. 2000 Rheology of ice at the bed of Engabreen, Norway. *J. Glaciol.* **46**(155), 611–621.
- Cuffey, K. M., Conway, H., Hallet, B., Gades, T. M. & Raymond, C. F. 1999 Interfacial water in polar glaciers and glacier sliding at -17°C . *Geophys. Res. Lett.* **26**(6), 751–754.
- Dennis, J. E. & Schnabel, R. B. 1996 *Numerical methods for unconstrained optimization and nonlinear equations*. Philadelphia, PA: SIAM.
- Echelmeyer, K. A., Harrison, W. D., Larsen, C. & Mitchell, J. E. 1994 The role of margins in the dynamics of an active ice stream. *J. Glaciol.* **40**(136), 527–538.
- Fowler, A. C. 1977 Glacier dynamics. DPhil thesis, University of Oxford, UK.
- Fowler, A. C. 1979 A mathematical approach to the theory of glacier sliding. *J. Glaciol.* **23**(89), 131–141.
- Fowler, A. C. 1981 A theoretical treatment of the sliding of glaciers in the absence of cavitation. *Phil. Trans. R. Soc. Lond.* **298**, 637–685.
- Fowler, A. C. 1986 A sliding law for glaciers of constant viscosity in the presence of subglacial cavitation. *Proc. R. Soc. Lond. A* **407**, 147–170.
- Fowler, A. C. 1987 Sliding with cavity formation. *J. Glaciol.* **33**(105), 255–267.
- Fowler, A. C. & Larson, D. A. 1978 On the flow of polythermal glaciers. I. Model and preliminary analysis. *Proc. R. Soc. Lond. A* **363**, 217–242.
- Gudmundsson, G. H. 1997 Basal-flow characteristics of a non-linear flow sliding frictionless over strongly undulating bedrock. *J. Glaciol.* **43**(143), 80–89.
- Holmes, M. H. 1995 *Introduction to perturbation methods*. Springer.
- Hubbard, B., Siegert, M. J. & McCarrroll, D. 2000 Spectral roughness of glaciated bedrock geomorphic surfaces: implications for glacier sliding. *J. Geophys. Res. B* **105**(9), 21 295–21 303.

- Hutter, K. 1983 *Theoretical glaciology*. Dordrecht: Reidel.
- Iken, A. 1981 The effect of subglacial water pressure on the sliding velocity of a glacier in an idealized numerical model. *J. Glaciol.* **27**(97), 407–422.
- Kamb, B. 1970 Sliding motion of glaciers: theory and observation. *Rev. Geophys.* **8**(4), 673–728.
- Kamb, B., Raymond, C. F., Harrison, W. D., Engelhardt, H., Echelmeyer, K. A., Humphrey, N., Brugman, M. M. & Pfeffer, T. 1985 Glacier surge mechanism: 1982–1983 surge of Variegated Glacier, Alaska. *Science* **227**(4686), 469–479.
- Liboutry, L. 1968 General theory of subglacial cavitation and sliding of temperate glaciers. *J. Glaciol.* **7**(49), 21–58.
- Liboutry, L. 1987 Realistic, yet simple bottom boundary conditions for glaciers and ice sheets. *J. Geophys. Res.* **B92**(9), 9101–9110.
- Morland, L. W. 1976a Glacier sliding down an inclined wavy bed. *J. Glaciol.* **17**(77), 447–462.
- Morland, L. W. & Johnson, I. R. 1980 Steady motion of ice sheets. *J. Glaciol.* **25**(92), 229–246.
- Morland, L. W., 1976b Glacier sliding down an inclined wavy bed with friction. *J. Glaciol.* **17**(77), 463–478.
- Muskhelishvili, N. I. 1953 *Singular integral equations*. Groningen: Noordhoff.
- Nye, J. F. 1969 A calculation of the sliding of ice over a wavy surface using a Newtonian viscous approximation. *Proc. R. Soc. Lond. A* **311**, 445–467.
- Nye, J. F. 1970 Glacier sliding without cavitation in a linear viscous approximation. *Proc. R. Soc. Lond. A* **315**, 381–403.
- Paterson, W. S. B. 1994 *The physics of glaciers*, 3rd edn. Oxford: Pergamon.
- Pattyn, F. 2002 Transient glacier response with a higher-order numerical ice-flow model. *J. Glaciol.* **48**(162), 467–477.
- Pollard, S. 1923 On the conditions for Cauchy's theorem. *Proc. Lond. Math. Soc.* **21**, 456–482.
- Raymond, C. 1996 Shear margins in glaciers and ice sheets. *J. Glaciol.* **42**(140), 90–102.
- Schoof, C. 2002a Basal perturbations under ice streams: form drag and surface expression. *J. Glaciol.* **48**(162), 407–416.
- Schoof, C. 2002b Mathematical models of glacier sliding and drumlin formation. DPhil. thesis, Oxford University, UK. (Available at <http://www.maths.ox.ac.uk/research/theses/>.)
- Schoof, C. 2005 On the mechanics of ice-stream shear margins. *J. Glaciol.* **50**. (In the press.)
- Schweizer, J. & Iken, A. 1992 The role of bed separation and friction in sliding over an undeformable bed. *J. Glaciol.* **38**(128), 77–92.
- Truffer, M. & Iken, A. 1998 The sliding velocity over a sinusoidal bed at high water pressure. *J. Glaciol.* **44**(147), 379–382.
- Truffer, M., Echelmeyer, K. A. & Harrison, W. D. 2001 Implications of till deformation on glacier dynamics. *J. Glaciol.* **47**(156), 123–134.
- Tulaczyk, S., Kamb, W. B. & Engelhardt, H. F. 2000a Basal mechanisms of Ice Stream B, West Antarctica. 1. Till mechanics. *J. Geophys. Res.* **B105**(1), 463–481.
- Tulaczyk, S., Kamb, W. B. & Engelhardt, H. F. 2000b Basal mechanisms of Ice Stream B, West Antarctica. 2. Undrained plastic bed model. *J. Geophys. Res.* **B105**(1), 483–494.
- Vivian, R. & Bocquet, G. 1973 Subglacial cavitation phenomena under Glacier d'Argentière, Mont Blanc, France. *J. Glaciol.* **12**(66), 439–452.
- Weertman, J. 1957 On the sliding of glaciers. *J. Glaciol.* **3**(21), 33–38.
- Weertman, J. & Birchfield, G. E. 1982 Subglacial water flow under ice streams and West Antarctic ice-sheet stability. *Ann. Glaciol.* **3**, 316–320.